The Astrophysical Journal, 644:560–564, 2006 June 10

STRONG INFRARED EMISSION FROM THE EXTRASOLAR PLANET HD 189733b

Drake Deming
Planetary Systems Laboratory, NASA Goddard Space Flight Center, Mail Code 693, Greenbelt, MD 20771; ddeming@pop600.gsfc.nasa.gov

Joseph Harrington
Center for Radiophysics and Space Research, Cornell University, 326 Space Sciences Building, Ithaca, NY 14853-6801; jh@oobleck.astro.cornell.edu

Sara Seager
Department of Terrestrial Magnetism, Carnegie Institution of Washington, 5241 Broad Branch Road NW, Washington, DC 20015; seager@dtm.ciw.edu

and

L. Jeremy Richardson[1]
Exoplanets and Stellar Astrophysics Laboratory, NASA Goddard Space Flight Center, Mail Code 667, Greenbelt, MD 20771; richardsonlj@milkyway.gsfc.nasa.gov

Received 2005 December 20; accepted 2006 February 3

ABSTRACT

We report detection of strong infrared thermal emission from the nearby ($d = 19$ pc) transiting extrasolar planet HD 189733b by measuring the flux decrement during its prominent secondary eclipse. A 6 hr photometric sequence using *Spitzer's* infrared spectrograph in peak-up imaging mode at 16 μm shows the secondary eclipse depth to be $0.551\% \pm 0.030\%$, with accuracy limited by instrumental baseline uncertainties, but with 32 σ precision ($\sigma = 0.017\%$) on the detection. The 16 μm brightness temperature of this planet (1117 ± 42 K) is very similar to the *Spitzer* detections of TrES-1 and HD 209458b, but the observed planetary flux (660 μJy) is an order of magnitude greater. This large signal will allow a detailed characterization of this planet in the infrared. Our photometry has sufficient signal-to-noise ratio ($\sim$400 per point) to motivate a search for structure in the ingress/egress portions of the eclipse curve, caused by putative thermal structure on the disk of the planet. We show that by binning our 6 s sampling down to $\sim$6 minute resolution, we detect the modulation in the intensity derivative during ingress/egress due to the overall shape of the planet, but our sensitivity is not yet sufficient to distinguish between realistic models of the temperature distribution across the planet's disk. We point out the potential for extending *Spitzer* secondary eclipse detections down to the regime of transiting hot Neptunes, if such systems are discovered among nearby lower main-sequence stars.

Subject headings: infrared: general — planetary systems — stars: individual (HD 189733)

Online material: machine-readable table

1. INTRODUCTION

The detection of infrared (IR) thermal emission from two extrasolar planets (Charbonneau et al. 2005; Deming et al. 2005) using the *Spitzer Space Telescope* (Werner et al. 2004) opened a new era in which planets orbiting other stars can be studied directly. The *Spitzer* detections were made by observing the flux decrement during secondary eclipse in transiting systems. The recently discovered planet transiting the star HD 189733 (Bouchy et al. 2005) is particularly suitable for *Spitzer* detection and characterization, because it transits a relatively small star—allowing maximum planet-star contrast—and because the distance to the system is only 19 pc (Perryman et al. 1997). HD 189733b has an orbital period of only 2.219 days (Bouchy et al. 2005), putting it in the class of "very hot Jupiters." Gaudi et al. (2005) suggested that the very hot Jupiters are a separate dynamical class of exoplanets. Since the other members of this class orbit much fainter stars, the discovery of HD 189733 may allow a previously impossible direct comparison between different classes of extrasolar planets.

In this paper we report detection of a prominent secondary eclipse of HD 189733b using *Spitzer* observations at 16 μm. We confirm that the strong IR thermal emission from this planet will indeed permit detailed characterization studies. To begin such studies, we examine our data for structure in the ingress/egress portions of the eclipse curve, as can be caused by temperature structure on the disk of the planet. We thus attempt the first exploratory observations of spatially resolved structure on the disk of a planet orbiting another star.

2. OBSERVATIONS

Whereas the first *Spitzer* detections (Charbonneau et al. 2005; Deming et al. 2005) were made using the IRAC and MIPS instruments, we here use the Infrared Spectrograph (IRS; Houck et al. 2004) in the peak-up imaging (PUI) mode to detect HD 189733b. This mode provides imaging photometry at a wavelength (16 μm peak, $\sim$5 μm FWHM) intermediate between the 8 μm IRAC and 24 μm MIPS bands. Our PUI photometry began on 2005 November 17 at 23:54 UTC. We placed the star alternately at two positions on the detector array, separated by 25″(13.5 pixels). We obtained 15 6 s exposures of the star at each position, then nodded to the other position, and repeated this cycle 98 times. We thus acquired a total of 1470 images during the 6 hr observation. The nod procedure allowed us to examine the zodiacal background at each position, out of phase

[1] NRC Postdoctoral Research Fellow.

with the stellar observations. This permits us to check the flat-fielding, using the spatially uniform background. The nod also permits measurement of latent image effects, and it provides insurance against unanticipated hot or inoperative pixels.

3. ANALYSIS

3.1. *Photometry*

The 16 μm zodiacal background in our observations of HD 189733 is approximately 9 MJy sr^{-1}, and this is sufficiently weak compared to HD 189733 (peak intensity $\sim$250 MJy sr^{-1}) to allow simple aperture photometry, not limited by background noise. After eliminating five images having obvious flaws, we summed the intensity for each image in a 9×9 pixel box centered on the star and subtracted the background level. The background level for each image was determined from a histogram of the pixel values outside of the stellar box, fitting a Gaussian to determine the centroid of the histogram. Photometry from the two nod positions differed by a constant factor close to unity (1.005) but showed no other differences above the noise. We normalized the measurements at both nod positions so as to yield the same average intensity.

We also performed aperture photometry on 2MASS 20004297+2242342, which is 11″ distant and about 4 mag fainter than HD 189733. We set the boundary of the 3×3 pixel box for this comparison star at the intensity minimum between the overlapping PSF wings of both stars. The comparison star contributes a very small flux in the photometry aperture for HD 189733 ($\sim$0.5%), and we corrected for this using a modeled *Spitzer* PSF.

Figure 1 shows the stellar photometry versus time for HD 189733 before background subtraction. We record about 10^6 electrons in each exposure, of which $\sim 6.3 \times 10^5$ are from the star. We therefore expect the stellar signal-to-noise ratio (S/N) to be $(6.3 \times 10^5)/10^3 = 630$. The point-to-point scatter in our final photometry is $\sim$0.0025, S/N $\sim$400. We were not able to improve this significantly by decorrelating against other parameters. For example, we found no significant correlation between the photometric noise and fluctuations in the position of the star on the detector (typically $\sim$0.05 pixels, $\sim$0.″1).

The S/N of our photometry is $\sim$60% of the photon noise limit, which is more than sufficient to detect the secondary eclipse of the planet. The eclipse is already obvious as the dip in the time series on Figure 1. A vertical line on the figure at phase 0.5 marks the nominal center of the eclipse. The reality of the eclipse is established by the fact that it is not present in either the comparison star or the background time series. Moreover, the amplitude, central phase, and shape of the eclipse are in close accord with expectations.

3.2. *Baseline Fitting*

Figure 1 shows that the measured intensity of the star increases steadily over the 6 hr observation sequence. Both the comparison star and the background level show a similar increase, which we denote as the "ramp." There are two peak-up arrays in IRS, and the red (22 μm) array (that was pointed to adjacent sky) shows a similar ramp. This ramp is a previously unreported instrument effect, not yet understood by the IRS instrument team. In 2005 July we observed two secondary eclipses of HD 209458 using IRS in the 7–14 μm spectroscopic mode. During these spectroscopic observations, the peak-up arrays (always operating) were both observing adjacent sky, and the background in all cases exhibits a similar ramp. We verified that the ramp appears in raw data, so it cannot be an artifact of the pipeline processing at the SSC. We detect very weak latent images

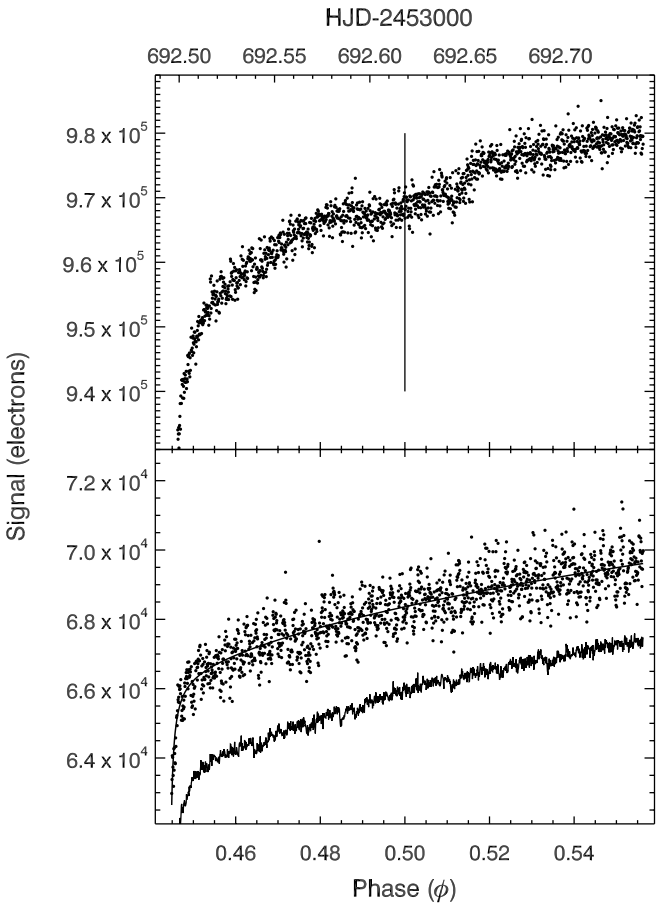

FIG. 1.—*Top*: Raw aperture photometry, before background subtraction and baseline correction, for HD 189733 vs. planetary phase. Note that the secondary eclipse is already visible near phase 0.5 marked by the vertical line. *Bottom*: Aperture photometry of the comparison star (2MASS 20004297+2242342; *points*), with a polynominal fit (*solid line through points*; see text). The line below the comparison star shows the background level, which has been increased by an arbitrary factor to place it on the same scale. The background in the HD 189733 aperture is about 30% of the total signal, and for the comparison star about 60%.

after changing the position of HD 189733, but their maximum amplitude ($\sim$0.002 of the real image) is not sufficient to account for the ramp. It should eventually be possible to diagnose the nature of this ramp and perhaps correct it from first principles. However, the secondary eclipse is of immediate interest, so here we fit a polynominal to the baseline.

The limiting factor in the accuracy of our secondary eclipse measurement is our ability to correct the ramp and establish an accurate photometric baseline spanning the eclipse. The ramp has a shape reminiscent of $y \propto \ln(\delta t)$, where δt is the elapsed time from start of observations, but a first-order log function does not fit it particularly well. Moreover, the shape of the ramp is slightly different for sources of different brightness (background, star).

To correct the baseline, we first divide background-subtracted HD 189733 photometry by the comparison star. We do not subtract background from the comparison star, so that it will be a closer match to the intensity level of HD 189733 and also will have greater S/N. It is still necessary to smooth the comparison star photometry, which we do by fitting a fourth-order polynominal in $\ln(\delta t)$ (Fig. 1). Dividing HD 189733 by this fit removes virtually all of the higher order curvature from the HD 189733 time series, for phases greater than 0.45 (neglecting the

TABLE 1
PHOTOMETRY BEFORE AND AFTER BASELINE CORRECTION

Observation Number	HJD 2,453,000	Phase	Signal (electrons)	Relative Intensity[a]
1.....	692.49608	0.44488	609247	0.0
2.....	692.49624	0.44495	610846	0.0
3.....	692.49639	0.44502	611768	0.0

NOTES.—Table 1 is published in its entirety in the electronic edition of the Astrophysical Journal. A portion is shown here for guidance regarding its form and content.

[a] Baseline-corrected, but given only for phase greater than 0.45.

strongly varying initial measurements). A residual ramp remains in HD 189733 after the division, but it is nearly linear. We zero-weight the eclipse itself ($0.482 \leq \phi \leq 0.518$), and we fit both a linear and a quadratic baseline to the residual ramp in the HD 189733 data.

Our baseline correction has the distinct advantage of not fitting a higher order polynominal directly to HD 189733 data. Because the eclipse itself must be zero-weighted, the higher order coefficients would have to be fit "over the gap," a less robust procedure that we avoid. For investigators who wish to do their own baseline corrections, we include an electronic table (Table 1) giving our photometry both before and after baseline correction. The original data are freely available from the *Spitzer* Science Center.

4. RESULTS AND DISCUSSION

4.1. *Stellar Flux*

Our background-subtracted photometry yields a stellar flux of 127 ± 8 mJy for HD 189733 at 16 μm. We included an aperture correction of 14%, calculated using a 24 μm MIPS PSF[2] scaled to 16 μm. Our flux error is from calibration scatter described in the IRS Data Handbook.[3] Interpolating in a grid of Kurucz model atmospheres, the flux expected from a 5050/4.5/0.0 model (Bouchy et al. 2005) at 19.3 pc is 104 mJy. The 2MASS K magnitude (=5.54) used with the STAR-PET calculator on the SSC Web site, for spectral type K2, predicts a stellar flux of 120 mJy. Given the difference between the 16 μm fluxes expected from the 2MASS magnitude, and from a Kurucz model for the Bouchy et al. (2005) temperature, there is no convincing evidence for a circumstellar dust contribution to the 16 μm flux. We therefore interpret the contrast in the secondary eclipse solely in terms of the planet-to-star flux ratio.

4.2. *Amplitude of the Secondary Eclipse*

Figure 2 shows the baseline-corrected secondary eclipse. We generate a theoretical eclipse curve numerically (Richardson et al. 2006) from the Bouchy et al. (2005) parameters for the system. We fit this to the individual measurements (Fig. 2, *top*). The fit has only two free parameters: phase at center of eclipse, and the eclipse depth. We estimate errors by generating and fitting to 10^4 fake data sets having $\sigma = 0.0025$, matching the scatter in the real data. The standard deviations of the eclipse depth and central phase from these Monte Carlo realizations are adopted as the errors for these parameters. The best-fit eclipse depth is $0.551\% \pm 0.017\%$, with central phase 0.5026 ± 0.0003. Adopting a stellar flux of $\sim$120 mJy, the flux from the planet is $\sim$660 μJy.

[2] See http://ssc.spitzer.caltech.edu/mips/psf.html.
[3] See http://ssc.spitzer.caltech.edu/irs/dh.

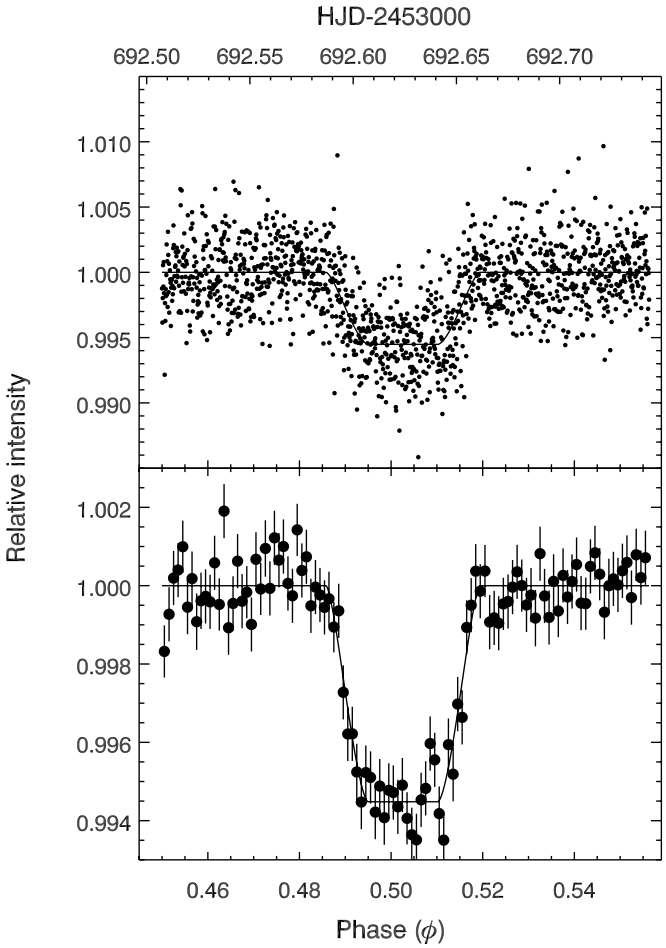

FIG. 2.—*Top*: Baseline-removed aperture photometry of the HD 189733 secondary eclipse. Points are individual 6 s measurements, with error bars suppressed for clarity, but showing the eclipse curve having the best-fit amplitude ($0.551\% \pm 0.03\%$) and central phase. *Bottom*: Data from the upper panel averaged in bins of width 0.001 in phase ($\sim$3 minutes), with error bars and the best-fit eclipse curve.

The exact eclipse depth is dependent on the details of the baseline correction. If we adopt a linear fit over the gap (see above), the derived eclipse depth is 0.521%. The choice between the linear and quadratic baselines is largely subjective; we prefer the quadratic baseline. The magnitude of the difference in eclipse depth for the two choices is indicative of the accuracy of our result, estimated as $\pm 0.03\%$. This being greater than the precision of the detection, baseline correction is the limiting factor in our analysis.

The lower panel of Figure 2 averages the photometry into bins of 0.001 in phase. The eclipse in the binned data is dramatic, and its duration and shape agree well with the theoretical curve. We are aware that some ground-based transit photometry for this planet yields a smaller radius (D. Charbonneau & G. Bakos 2005, private communication). However, the duration of secondary eclipse should be the same as the transit duration, already relatively well determined by the discovery observations. We do not expect that a smaller radius for the planet will affect the duration and shape of the secondary eclipse curve by more than our errors. The brightness temperature inferred for the planet may be more sensitive to radius (see below).

The central phase of the eclipse, 0.5026 ± 0.0003, is seemingly different from 0.5, and at face value this would indicate a noncircular orbit. However, the difference between the discovery

orbital period, 2.219 days (Bouchy et al. 2005), and the *Hipparcos* value we used (2.218575 days; Hebrard & Lecavelier des Estangs 2006; Bouchy et al. 2005), when propagated to the time of our observations, give a phase difference (0.0046) that is greater than the offset we observe. Therefore, we regard any conclusions about the central phase of the eclipse as premature until the ephemeris is more firmly established. For reference, our secondary eclipse is centered at HJD = 2453692.62416 ± 0.00067. Unlike the eclipse depth, the center time does not depend significantly on our baseline correction.

It is interesting to compare this planet with the *Spitzer* detection of TrES-1 (Charbonneau et al. 2005), since both planets orbit K dwarfs. In thermal equilibrium, and assuming equal Bond albedos and heat redistribution efficiencies for both planets, their temperatures will scale as

$$T_p \sim T_s \Delta^{1/2}, \quad (1)$$

where T_s is the effective temperature of the star and Δ is its angular diameter as seen from the planet. For the TrES-1 (Alonso et al. 2004; Sozetti et al. 2004) and HD 189733 parameters (Bouchy et al. 2005), equation (1) predicts virtually identical temperatures, as the larger and hotter star has the more distant planet (TrES-1). The 16 μm brightness temperature of HD 189733, from a Kurucz model, is 4315 K. Adopting the Bouchy et al. (2005) ratio of radii, our secondary eclipse contrast translates to a 16 μm brightness temperature for the planet of 1117 ± 42 K. This is very similar to both the TrES-1 (1060 ± 50 K; Charbonneau et al. 2005) and HD 209458b (1130 ± 150 K; Deming et al. 2005) detections. Our contrast measurement is in close accord with a prediction for HD 189733b by Fortney et al. (2006), who expect HD 189733b to be intermediate between TrES-1 and HD 209458b. However, if the planet-to-star radius *ratio* for HD 189733 is revised, then our revised brightness temperature will be

$$T_p^{16} = 900/\ln\left(1 + 41.86r^2\right), \quad (2)$$

where r is the ratio of planet radius to the stellar radius. Our 16 μm measurement is as close to a continuum flux as possible using *Spitzer* photometry; comparison with the IRAC and MIPS (24 μm) bands (DDT program 261 by D. Charbonneau) should define the degree of absorption by methane, water, and CO (Seager et al. 2005; Fortney et al. 2006).

4.3. *Beyond the Eclipse Amplitude*

The fact that *Spitzer* detects this secondary eclipse to high S/N (32 σ precision) prompts us to ask what other information can be extracted from the eclipse curve and what the implications are for the detection of lower mass planets, for example, hot Neptunes (Bonfils et al. 2005) that may transit.

The bottom panel of Figure 2 suggests that our binned data during ingress and egress contain information on the shape of the eclipse curve. The pressure scale height in the atmosphere of a solar type star (Vernazza et al. 1976) is much less than the radius of a planet. Hence, the shape of the secondary eclipse curve encodes information on the spatial distribution of IR intensity across the planet's disk (Charbonneau et al. 2005). We computed the derivative of intensity with respect to time (phase) for our binned data. We approximate the derivatives as simple finite differences. We fold the eclipse curve about mideclipse, averaging ingress and egress, before computing derivatives. Folding maximizes our sensitivity but smears any planetary thermal structure that is not symmetric.

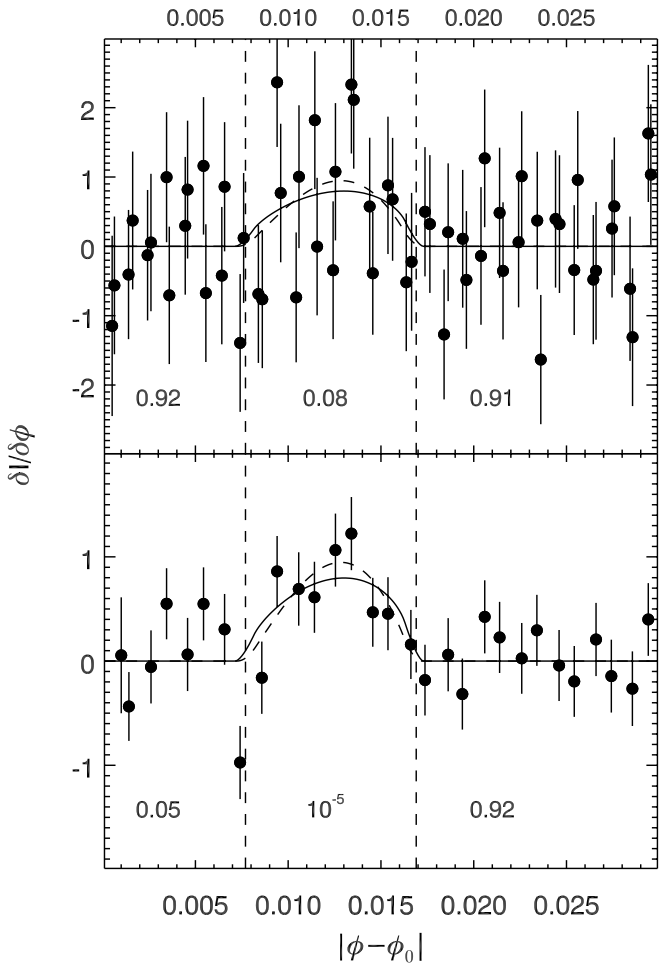

FIG. 3.—*Top*: Derivative of relative intensity during eclipse with respect to phase (ϕ) vs. the absolute phase difference from the center of eclipse (ϕ_0). The derivative values from the data were obtained using a phase resolution of 0.001. The dashed vertical lines indicate the start and end of ingress and egress. *Bottom*: Derivative of relative intensity vs. phase, as in top panel, but for a phase resolution of 0.002. The curved line shows the relation expected for a circular planet of uniform brightness temperature, and the dashed line has a temperature distribution sharply peaked at the planet's disk center. The numbers in each region of the figure are the probabilities, from a χ^2 analysis, that the observed derivatives are consistent with zero.

Figure 3 shows the results for two bin sizes: 0.001 in phase (*top panel*) and 0.002 (*bottom panel*). At 0.001 resolution (=3 minutes) the scatter is much greater than the amplitude of the derivative curve, but the average derivative during ingress/egress is higher than at other phases. As we increase the bin size, the derivatives during ingress/egress must inevitably become significantly different from zero. This follows because the integral of the derivative is the eclipse curve itself, which is already detected to high significance. At 0.002 resolution (6 minutes), the scatter is dramatically improved, the derivatives peak near mid-ingress/egress, and a χ^2 analysis firmly rejects the null hypothesis that the derivatives are consistent with zero (10^{-5} probability). A similar analysis for the comparison star finds only random noise. Apart from the real derivative increase during ingress/egress, only the lower left bin on Figure 3 stands out in the χ^2 analysis, with a 5% probability of being due to noise. This marginal value is due to the extra noise noticeable just before egress, rather than to a real derivative signal. The extra noise can also be seen in the background fluctuations at this time (see Fig. 1).

Figure 3 compares the observed derivatives to models that are constrained to fit the observed eclipse depth. We use two simple, ad hoc models: a uniform brightness temperature on the disk (*solid line*), and an extreme limb-darkened model with intensity falling proportional to cos (θ), becoming zero at the limb (*dashed line*). The dominant effect in the modeled and observed derivatives is the shape of the planet. At 6 minute resolution, the individual derivatives peak at the middle of ingress/egress. The data crudely indicate the overall shape of the planet but cannot discriminate between a uniform disk (*solid line*) and the extreme limb-darkened model (*dashed line*). However, modest improvements in the *Spitzer* duty cycle and S/N may allow us to relax our symmetry assumption and place meaningful limits on dynamically forced temperature asymmetries of large spatial scale on the planet's disk (Cho et al. 2003; Cooper & Showman 2005).

The 32 σ precision we obtain for this secondary eclipse remains a >3 σ detection for a planet an order of magnitude smaller in area but in an identical orbit. This limit corresponds to $\sim$1 Neptune radius. As we proceed down the main sequence, planet-to-star contrast increases as the inverse square of the stellar radius. For planets orbiting M dwarfs (Bonfils et al. 2005; Rivera et al. 2005; Butler et al. 2004), it follows from equation (1) that, in the Rayleigh-Jeans limit, this dominates the reduced heating of the planets. If close-in Neptunes are discovered transiting nearby M dwarfs, their IR emission should be detectable by *Spitzer*.

This work is based on observations made with the *Spitzer Space Telescope*, which is operated by the Jet Propulsion Laboratory, California Institute of Technology, under a contract with NASA. Support for this work was provided by NASA. We thank Gordon Squires for his rapid handling of our proposal, and the entire *Spitzer* staff for their efficient scheduling and rapid data processing. We are grateful to Dave Charbonneau and Gaspar Bakos for discussions concerning this planet, and we thank Daniel Devost, Kevin Uchida, James Houck, and Gregory Sloan for their thoughts regarding IRS systematics. We thank an anonymous referee for comments that improved this paper.

REFERENCES

Alonso, R., et al. 2004, ApJ, 613, L15
Bonfils, X., et al. 2005, A&A, 443, L15
Bouchy, F., et al. 2005, A&A, 444, L15
Butler, R. P., Vogt, S. S., Marcy, G. W., Fischer, D. A., Wright, J. T., Henry, G. W., Laughlin, G., & Lissauer, J. J. 2004, ApJ, 617, 580
Charbonneau, D., et al. 2005, ApJ, 626, 523
Cho, J. Y.-K., Menou, K., Hansen, B. M. S., & Seager, S. 2003, ApJ, 587, L117
Cooper, C. S., & Showman, A. P. 2005, ApJ, 629, L45
Deming, D., Seager, S., Richardson, L. J., & Harrington, J. 2005, Nature, 552, 699
Fortney, J. J., Saumon, D., Marley, M. S., Lodders, K., & Freedman, R. S. 2006, ApJ, in press (astro-ph/0507422)
Gaudi, B. S., Seager, S., & Mallen-Ornelas, G. 2005, ApJ, 623, 472
Hebrard, G., & Lecavelier des Estang, A. 2006, A&A, 445, 341
Houck, J. R., et al. 2004, ApJS, 154, 18
Perryman, M. A. C., ed. 1997, The *Hipparcos* and Tycho Catalogues (ESA SP-1200; Noordwijk: ESA)
Richardson, J. L., Seager, S., Deming, D., Harrington, J., Barry, R. K., Rajagopal, J., & Danchi, W. C. 2006, in IAU Circ. 200, Direct Detection of Exoplanets: Science & Techniques, ed. C. Aime & F. Vakili, in press
Rivera, E. J., et al. 2005, ApJ, 634, 625
Seager, S., Richardson, L. J., Hansen, B. M. S., Menou, K., Cho, J. Y.-K., & Deming, D. 2005, ApJ, 632, 1122
Sozetti, A., et al. 2004, ApJ, 616, L197
Vernazza, J. E., Avrett, E. H., & Loeser, R. 1976, ApJS, 30, 1
Werner, M. W., et al. 2004, ApJS, 154, 1

Note added in proof.—A recent revision of the planet's radius by Bakos et al. raises the 16 μm brightness temperature at the planet to 1318 $\pm$ 104 K.